Trends in Southern Hemisphere Circulation in IPCC AR4 Models over 1950–99: Ozone Depletion versus Greenhouse Forcing

WENJU CAI AND TIM COWAN

CSIRO Marine and Atmospheric Research, Aspendale, Victoria, Australia

(Manuscript received 24 January 2006, in final form 13 July 2006)

ABSTRACT

Simulations by the Intergovernmental Panel on Climate Change (IPCC) Fourth Assessment Report (AR4) models on the Southern Hemisphere (SH) circulation are assessed over the period 1950–99, focusing on the seasonality of the trend and the level of its congruency with the southern annular mode (SAM) in terms of surface zonal wind stress. It is found that, as a group, the models realistically produce the seasonality of the trend, which is strongest in the SH summer season, December–February (DJF). The modeled DJF trend is principally congruent with the modeled SAM trend, as in observations. The majority of models produce a statistically significant positive trend, with decreasing westerlies in the midlatitudes and increasing westerlies in the high latitudes. The trend pattern from an all-experiment mean achieves highest correlation with that from the National Centers for Environmental Prediction (NCEP) data. A total of 48 out of the 71 experiments were run with ozone-depletion forcing, which offers an opportunity to assess the importance of ozone depletion in driving the late-twentieth-century trends. The AR4 model ensemble that contains an ozone-depletion forcing produces an averaged trend that is comparable to the trend from the NCEP outputs corrected by station-based observations. The trend is largely generated after the mid-1970s. Without ozone depletion the trend is less than half of that in the corrected NCEP, although the errors in the observed trend are large. The impact on oceanic circulation is inferred from wind stress curl in the group with ozone-depletion forcing. The result shows an intensification of the southern midlatitude supergyre circulation, including a strengthening East Australian Current flowing through the Tasman Sea. Thus, ozone depletion also plays an important role in the subtropical gyre circulation change over the past decades.

1. Introduction

The southern annular mode (SAM) is the dominant mode of the Southern Hemisphere (SH) extratropical circulation operating on all time scales (Kidson 1988; Karoly 1990; Thompson et al. 2000; Thompson and Solomon 2002; Hartmann and Lo 1998). Over the past decades strong changes in the SH circulation have occurred, largely projecting onto the SAM as a bias toward the high-index polarity (Kidson 1988; Karoly 1990; Hartmann and Lo 1998; Thompson et al. 2000). These changes feature a strengthening of the circumpolar westerly and a weakening of the midlatitude westerly extending from the stratosphere to earth's surface. In terms of the circumpolar westerlies, temperature, and geopotential height, the largest changes in the stratosphere have occurred during the spring months (Randel and Wu 1999; Waugh et al. 1999; Zhou et al. 2000; Thompson and Solomon 2002; Gillett and Thompson 2003); however, from the troposphere to the earth's surface, the summer months display the largest changes (Thompson and Solomon 2002; Gillett and Thompson 2003). This time lag was further elucidated using ozonesonde observations over the past 40 yr (Solomon et al. 2005).

Attribution of the causes for these changes is rather difficult because there is only one real-world realization. Therefore, much of the effort has to rely on climate models. Simulations conducted with increasing greenhouse gases produce trends that are of the same sign as the observed trend (Fyfe et al. 1999; Kushner et al. 2001; Cai et al. 2003), whereas the simulated trend without ozone-depletion forcing is considerably smaller than the observed (Sexton 2001; Shindell and Schmidt 2004). Based on observations, Thompson and Solomon (2002) argued that the summer trend is consistent with forcing by stratospheric ozone depletion and this was

Corresponding author address: Wenju Cai, CSIRO Marine and Atmospheric Research, 107 Station Street, Aspendale, VIC 3195, Australia.
E-mail: Wenju.Cai@csiro.au

DOI: 10.1175/JCLI4028.1

tested by Gillett and Thompson (2003), who concluded that the anthropogenic emissions of ozone-depleting gases primarily account for the observed trends of surface flows at the midlatitudes since the 1970s. Marshall et al. (2004) demonstrated that the trend starts before the ozone depletion commences, although this is not inconsistent with an ozone depletion–induced acceleration of the trend since the mid-1970s. All these efforts are limited in the sense that they use only one particular model. The consensus is that both ozone-depletion and greenhouse forcing have contributed to the observed trend; however, the varying partition from one model to another is likely to be because of individual models containing biases in their representation of the relative importance of each forcing.

Alleviating these biases requires detailed benchmarking of the climate models using observations, which are, however, largely void over the SH prior to the late 1970s. The research community relies heavily on reanalysis such as that from the National Centers for Environmental Prediction (NCEP; Kalnay et al. 1996), which unfortunately has spurious trends (Marshall 2003). A multimodel ensemble provides an excellent strategy because model errors of opposing nature will be nullified. A multimodel ensemble also reduces the contribution of unforced variability. Therefore, any conclusions based on multimodel ensemble averages are likely to be more reliable than perspectives from individual models.

The unprecedented number of simulations from the late nineteenth century through to the end of the twentieth century conducted by climate modeling groups worldwide as part of the Fourth Assessment Report (AR4) by the Intergovernmental Panel on Climate Change (IPCC) provides an opportunity for the ensemble strategy to be acted upon. One can make comparisons on the reliability of individual models to simulate observations by whether the models include an ozone-depletion forcing in their experiments. A realistic model simulation of this contribution is particularly important because ozone is projected to recover by the year 2050, and its impact will be opposite to that of increasing CO_2 on SH climate. Thus, if climate models underrepresent the impact of ozone depletion over the most recent decades, they will underestimate the opposing effect in the projection of future SH climate and vice versa.

Many recent studies have used the outputs of the AR4 models to address important issues. For example, Carril et al. (2005) explore the impact of the SAM trend on sea ice and temperature changes in the surroundings of the Antarctic Peninsula; Miller et al. (2006, manuscript submitted to *J. Geophys. Res.*, hereafter MSS) focus on the variability and trends of the SAM in terms of mean sea level pressure (MSLP) and assess the relative importance of ozone-depletion and greenhouse forcing, although they use only models that have more than one ensemble member. Raphael and Holland (2005) examine the simulation in five models of the SH variability. Yin (2005) analyzes the outputs of 15 coupled models in the twenty-first century in terms of changes in storm tracks in the SH. Fyfe and Saenko (2006) focus on the response of zonal mean flows, in particular, the response of the Antarctic Circumpolar Current (ACC), and examine the role of the associated Ekman transport change, which has the biggest effects on oceanic current where the wind change is largest, and find the ACC intensifies and shifts southward. Russell et al. (2006a) examine the impact of the intensifying westerlies on the heat storage, stratification, and ventilation of the Southern Ocean in the National Oceanic and Atmospheric Administration Geophysical Fluid Dynamics Laboratory (NOAA/GFDL) model. Arblaster and Meehl (2006) use the National Center for Atmospheric Research Parallel Climate Model Version 1 (NCAR PCM1) to show that ozone depletion is the greatest external forcing on the SH summertime circumpolar vortex intensification.

In the present study, we take advantage of all model experiments available and benchmark the trend of surface wind stress in terms of the seasonality and their congruency with the SAM in individual models. Previous observational analyses have shown that there is a strong seasonality in the trend and that most of the trend projects onto the SAM. These are important ingredients of the whole argument for the role of ozone depletion in driving the observed climate change in the SH, but the ability of AR4 models in simulating them has yet to be fully examined. The reason for focusing on surface wind stress is that there are few direct ocean measurements; therefore, oceanic trends will have to be assessed partially through surface wind changes. Particularly, we infer the trend of the subtropical gyre circulation, which is determined by wind stress curl changes integrated from an eastern boundary, not the local change of wind stress. Our work, therefore, provides a useful complement to diagnoses of temperature and sea ice by Carril et al. (2005), MSLP by MSS, the ACC by Fyfe and Saenko (2005, 2006), and the thermodynamics of the ocean response by Russell et al. (2006a).

For comparison, we use NCEP wind stress, which, however, is an ambiguous measure of the model fidelity because it is not directly measured. NCEP lists wind as a "class C" quantity (Table 4 of Kalnay et al. 1996),

TABLE 1. Model information.

Model	Country	Levels	20c3m	Ozone	Reference
CCCma T47	Canada	31	5	No	Flato et al. (2000)
CCCma T63	Canada	31	1	No	Flato et al. (2000)
CNRM CM3	France	48	1	Yes	Salas-Mélia et al. (2005, manuscript submitted to *Climate Dyn.*)
CSIRO Mk3.0	Australia	18	3	Yes	Gordon et al. (2002)
NOAA/GFDL CM2.0	United States	24	3	Yes	Delworth et al. (2006)
NOAA/GFDL CM2.1	United States	24	3	Yes	Delworth et al. (2006)
NASA GISS AOGCM	United States	12	2	No	Russell et al. (1995)
NASA GISS-EH	United States	20	5	Yes	Schmidt et al. (2006)
NASA GISS-ER	United States	20	9	Yes	Schmidt et al. (2006)
IAP FGOALS	China	26	3	No	Yu et al. (2004)
INM-CM3.0*	Russia	21	1	No	Diansky and Volodin (2002)
IPSL CM4	France	19	1	No	Marti et al. (2005)
MIROC(hires)	Japan	56	1	Yes	Hasumi and Emori (2004)
MIROC(medres)	Japan	20	3	Yes	Hasumi and Emori (2004)
MIUB ECHO*	Germany/Korea	30	5	No	Legutke and Voss (1999)
MPI ECHAM5	Germany	31	3	Yes	Jungclaus et al. (2006)
MRI CGCM2*	Japan	30	5	No	Yukimoto et al. (2005)
NCAR CCSM3.0	United States	26	9	Yes	Meehl et al. (2006)
NCAR PCM1	United States	18	4	Yes	Washington et al. (2000)
UKMO HadCM3	United Kingdom	19	2	Yes	Gordon et al. (2000)
UKMO HadGEM1	United Kingdom	38	2	Yes	Johns et al. (2005)

* Models experiments contain flux adjustments (available online at http://www-pcmdi.llnl.gov/).

because it is calculated using a planetary boundary layer (PBL) parameterization. As such, any disagreement of a model with NCEP may reflect true model errors or it may result from unrealistic behavior by the PBL parameterization in the reanalysis model. Nevertheless, as we will show, in terms of the trend over the past 50 yr, once the spurious trend discussed by Marshall (2003) is corrected, a reasonable agreement is achieved between the group with ozone depletion and the corrected NCEP wind stress. Using a well-established wind-driven ocean circulation model (Godfrey 1989) forced by observed and modeled future changes in surface winds, Cai et al. (2005) and Cai (2006) demonstrate the SAM can significantly impact on the SH subtropical gyre circulation and on the marine ecosystem. We will use the trends in surface wind stress curl to estimate gyre circulation change and assess the importance of ozone depletion in driving this change over the past 50 yr.

It is appropriate to note that while we focus on the trends, several studies have identified some bias in the mean climate of the AR4 models. Fyfe and Saenko (2006, their Fig. 2) find that the simulated zonal wind is significantly too equatorward especially over the Pacific Ocean. Russell et al. (2006b, their Fig. 3) show that the magnitude and position SH zonal wind is significantly in error, which in turn affects other aspects of the simulation (e.g., oceanic heat uptake); their comprehensive examination of these aspects of the Southern Ocean mean circulation—for example, the ACC, the overturning, and water mass properties—provides important, useful information.

In what follows, we briefly describe the AR4 models (section 2) before focusing on the seasonality of the trend, the level of congruency with the SAM, and the statistical significance of the trends in individual models and in the all experiment mean (AEM; the AEM consists of all 71 experiments, regardless of whether they contain ozone or not). We then compare the model results with outputs from NCEP reanalysis and examine the importance of ozone depletion (section 4) in wind and the implied ocean gyre circulation changes.

2. Model and experiment details

We analyze 21 IPCC AR4 coupled general circulation model (CGCM) simulations composing a total of 71 runs that include surface wind stress data for the twentieth-century climate experiment (20c3m). The model data were made available through the U.S. Department of Energy's Program for Climate Model Diagnosis and Intercomparison (PCMDI). Each model is listed in Table 1, with a reference to further documentation. Model group acronym meanings can be found in Table 2. In addition it must be noted that certain models contain similarities, for example, the National Aeronautics and Space Administration (NASA) Goddard Institute for Space Studies Model E-H and Model E-R

TABLE 2. Model acronyms.

Model	Scientific organization
CCCma	Canadian Center for Climate Modelling and Analysis
CNRM	Centre National de Recherches Météorologiques, Météo-France
CSIRO	Commonwealth Scientific and Industrial Research Organisation
NOAA/GFDL	National Oceanic and Atmospheric Administration/Geophysical Fluid Dynamics Laboratory
NASA GISS	National Aeronautics and Space Administration Goddard Institute for Space Studies
IAP	Institute of Atmospheric Physics
INM	Institute for Numerical Mathematics
IPSL	Institut Pierre Simon Laplace
MIROC	Model for Interdisciplinary Research on Climate
MIUB	Meteorological Institute of the University of Bonn
MPI	Max Planck Institute for Meteorology
MRI	Meteorological Research Institute
NCAR	National Center for Atmospheric Research
UKMO Had	Met Office/Hadley Centre for Climate Prediction and Research

(GISS-EH, GISS-ER), while featuring identical atmospheric model, do not share the same ocean component (Collins et al. 2006; MSS).

All the models contain greenhouse gas and direct sulfate aerosol forcing, whereas 13 out of the 21 models include a stratospheric ozone forcing component. The number of 20c3m model runs range from 1 to 9, with 13 out of the 21 models contributing 3 or more experiment runs. A large proportion of the models were run without flux adjustments (see Table 1). The horizontal resolution varies from one model to another, ranging from high {1.125° × 1.125° for Model for Interdisciplinary Research on Climate, high-resolution version [MIROC(hires)]} to coarse [4° × 5° for Institute of Numerical Mathematics Coupled Model version 3.0 (INM-CM3.0)]. To facilitate an AEM, each model's results are interpolated onto a common grid, which, for convenience, is chosen to be 3.75° × 3.75°. Through a weighted average we remove any likelihood that models with a low number of experiments are overly represented. The weighted average is calculated by multiplying each model by the number of experiments used and dividing through the sum by the total number of all model experiments. We will also discuss results from an alternative approach, that is, all model average regardless of the ensemble member of a model.

To evaluate the performance of the models and their ensemble, observational data from the NCEP reanalysis are used. It has been shown in previous studies (Marshall 2003) that the raw NCEP MSLP produces a SAM trend that is too large. To correct this overestimate in the trend we perform a regression of the NCEP zonal wind stress onto an observed station-based index of the SAM (Marshall 2003). We use a non-normalized SAM index defined as the difference in zonally averaged MSLP between 40° and 65°S, because we are interested in the absolute trends. As such, for the remainder of the paper we will refer to NCEP as being corrected to station observations, unless otherwise stated. We focused much of our attention on the SH summer (December–February), as this is the period when the trend is strongest.

Empirical orthogonal function (EOF) spatial patterns and time amplitude functions (TAFs) are calculated in the domain of 20°–70°S. We use a covariance EOF, and the variance of the spatial pattern of an EOF sums to unity, leaving the trend and variance of an EOF to be recorded in the TAF. The time trend of an EOF can, therefore, be calculated from the corresponding TAF. Before application of EOF analysis the climatological mean, which is the average over the period 1950–99, is removed.

As will be clear, all models produce a SAM-like mode as their EOF1, but the structure of the associated spatial pattern varies significantly. Despite the difference, the SAM in each model is used to assess the trend and compared with the trend from the NCEP reanalysis. We note that this approach appears somewhat different from that of others (e.g., MSS), which uses the EOF1 from the ensemble mean as the SAM and then projects outputs from each model onto the ensemble mean EOF1 to construct a time series, from which the trend is then assessed. It turns out that both approaches allow the SAM in each model to contribute to the ensemble mean, and are little different.

3. Results

a. Seasonality of the trend

There is strong seasonality in the trend of the SH surface circulation over the period 1950–99. Using model results and station-based observations, Marshall (2003) showed that the trend in terms of MSLP is strongest in the southern summer and weakest in winter. We start by examining how well the models reproduce the seasonality. Figures 1a and 1b show the trends of the zonal wind stress AEM for December–February (DJF) and June–August (JJA). The models, as a group, reproduce the seasonality very well. In particular, the DJF trend at 60°S is about twice as large as the JJA trend and is more zonally symmetric. In both seasons,

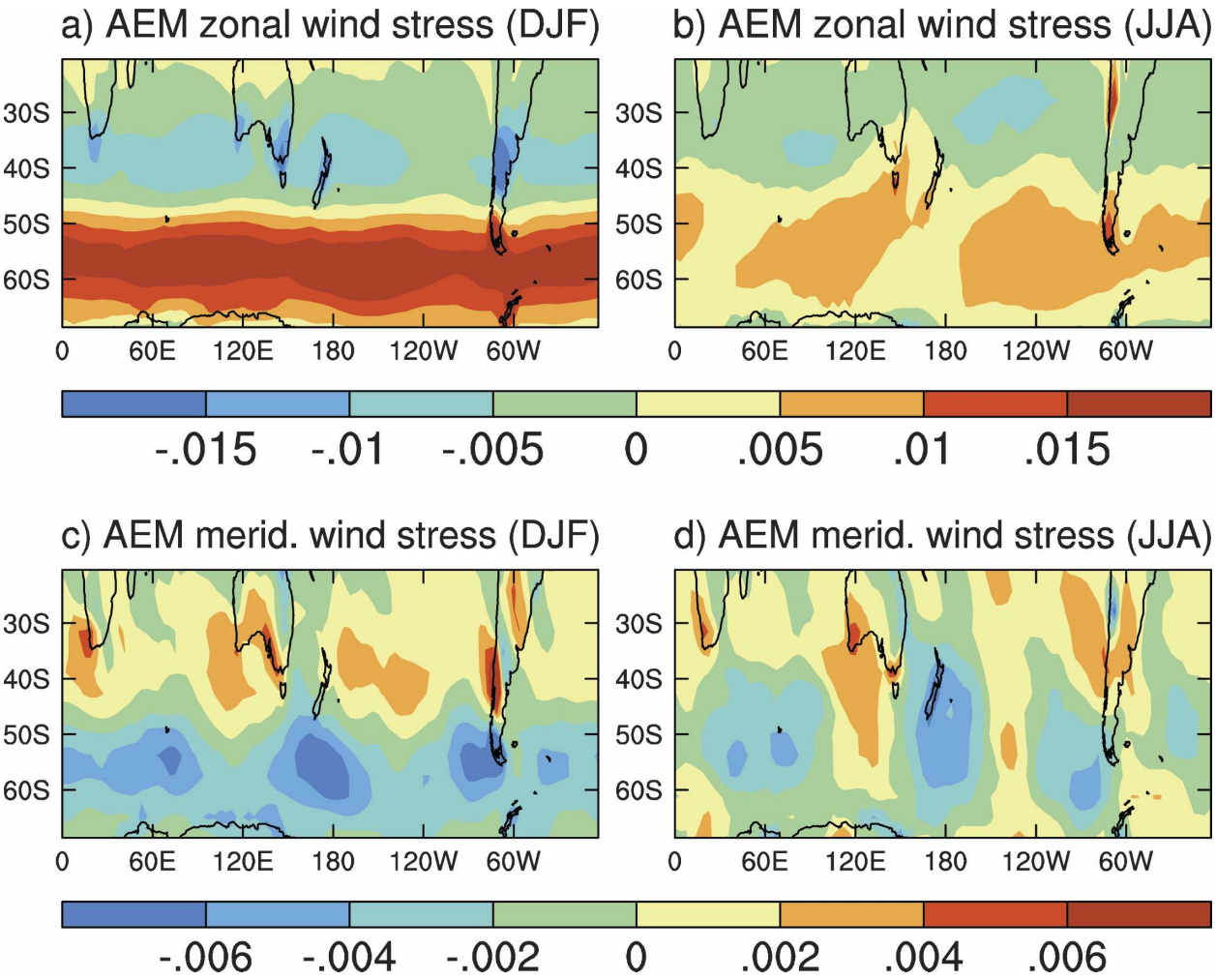

FIG. 1. Linear trend of AEM zonal wind stress: (a) DJF and (b) JJA. (c), (d) Same as in (a), (b), but for AEM meridional wind stress. Units: N m^{-2} per half century (1950–99). AEM is calculated by multiplying each model by the number of experiments used and dividing through the sum by the total number of all model experiments.

there are no well-defined trends of the northern annular mode (figure not shown), as discussed by MSS. In terms of meridional wind stress trends, again a more zonally symmetric pattern is seen in DJF (Fig. 1c) than in JJA (Fig. 1d).

There is a higher level of intermodel consistency for the trend pattern of DJF zonal wind stress than for the JJA structure. This reflects the fact that model trends are weaker in JJA than in DJF, so that internal model variability has a relatively larger effect in JJA. Coefficients of pattern correlation between the NCEP trend pattern with trend patterns of the individual models are plotted in Fig. 2 for DJF (circles) and JJA (squares). We have separated the models into those that contain ozone-depletion forcing and those that do not. In DJF, the pattern correlations are generally higher for the models that contain ozone forcing, whereas those without ozone tend to be at or below 0.6. The JJA structure is less well simulated with the majority of models scoring less than 0.5. The AEM performs the best in DJF and does reasonably well in JJA. However, even for DJF, not all models produce a positive correlation. The trend in the GISS atmosphere–ocean general circulation model (AOGCM), although rather weak, is actually opposite to that shown in Fig. 1a. We shall discuss this further.

A set of sample models that feature high and low correlation coefficients are shown in Fig. 3 for DJF (left column) and JJA (right column). They are compared to NCEP trends (top of each column). For DJF, it seems that the variation in the correlation coefficients mainly reflects the difference in the zonal structure, with a strongly varying level of zonal symmetry. For JJA, the overall zonal symmetry does not extend across the

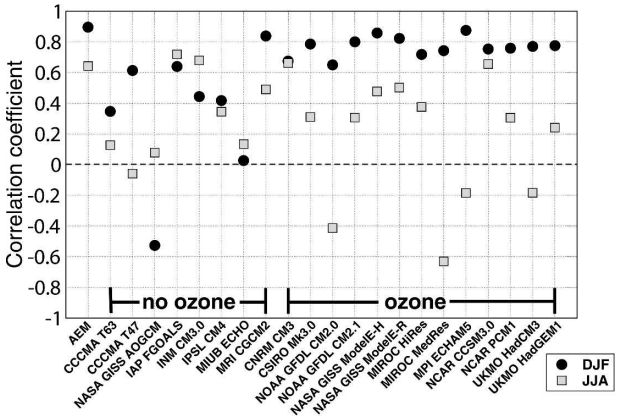

FIG. 2. Pattern correlation between the linear trend of corrected NCEP zonal mean wind stress and trend from each model for both DJF and JJA. The analysis is carried out in the domain of 20°–70°S, over the period 1950–99. NCEP trend pattern is from 1957 to 1999.

whole SH and the trend patterns differ greatly from one model to another.

One would expect that the AEM trend pattern would be more similar to that from the models with more ensemble members, for example, NCAR Community Climate System Model version 3 (CCSM3) and GISS-ER (each with nine ensemble members), but this is not necessarily the case. For example, in terms of DJF zonal wind stress, the highest individual model correlation is achieved for the Max Planck Institute for Meteorology European Centre-Hamburg Model version 5 (MPI ECHAM5), which has three ensemble members. Furthermore, models (with ozone) that contain three members or less achieve comparable pattern correlations. Thus, the number of experiments does not seem to dominate the AEM.

Similar pattern correlation analysis is conducted for meridional wind stress (not shown). In general, correlation coefficients between NCEP and individual model trends are lower than for the zonal wind stress, with none exceeding 0.6. Again the AEM performs the best in DJF with a correlation close to 0.6. Similarly, the ozone group as a whole is more highly correlated in DJF with NCEP than the non-ozone group, whereas there is no noticeable distinction in JJA between the ozone and non-ozone group, suggesting that ozone depletion has little impact on the trend in JJA.

b. Congruency with the SAM: The trend in terms of EOF

1) EOF1 OF ZONAL WIND STRESS

Previous studies have shown that much of the SH circulation trend is congruent with the SAM (Thompson and Solomon 2002; Marshall 2003). In what follows we test the ability of the AR4 models to simulate this feature. Since the trend is stronger in DJF we focus on this season. To this end EOF analysis is conducted in the domain of the SH (20°–70°S) on zonal wind stress. Implicitly we are defining the SAM in terms of zonal wind stress EOF1.

There are two approaches for examining the level of congruency with the SAM. One is to apply EOF to zonal wind stress in each model, calculate the trend from EOF1 in each model, and obtain an average of the trend weighted by each model's ensemble member. The other is to apply EOF to AEM zonal wind and calculate the trend in the EOF1. In either approach trends obtained are to be compared with the linear trends shown in Fig. 1. We find that the results from these two approaches are almost identical. Since the former allows assessment on the level of congruency in each individual model, it is adopted here.

In general, the modeled DJF EOF1 explains between 35% and 60% of the total variance, compared with that from raw NCEP of 34.7% of the total variance. MSS showed that the models generally overestimate SH variability of SLP and the SAM percentage of the total variance. In terms of zonal wind stress, the same conclusion applies.

The trend pattern from zonal wind stress EOF1 (Fig. 4a) shows a strong similarity to the linear trend (Fig. 1a) with a pattern correlation of 0.975. At most locations, the trend from EOF1 accounts for more than 90% of the trend in Fig. 1a, reinforcing the notion that most of the circulation trend is congruent with the SAM trend. The AEM time series of EOF1 (Fig. 5) shows an upward trend with a linear slope of 0.38 per 50 yr. Much of the trend starts in the mid-1970s. We will discuss this feature in section 4b.

The meridional wind pattern associated with the EOF1 of zonal wind stress (Fig. 4b), obtained through a linear regression onto the EOF1 time series of zonal wind stress (Fig. 5) and then multiplying the slope of the time series, resembles that of the linear trend shown in Fig. 1b with a pattern correlation of 0.96.

Patterns from each model are similar to that shown in Fig. 4a, with pattern correlation coefficients in the range of 0.60–0.95 (Fig. 6). The majority of models produce a coefficient greater than 0.9. Even for the GISS AOGCM, which shows a negative trend, the pattern correlation is high. The large coefficients mean that these models produce a SAM-like mode as the dominant mode of variability and that the trend is projected onto this mode.

The difference in EOF1 pattern from one model to another mainly reflects the difference in the meridional

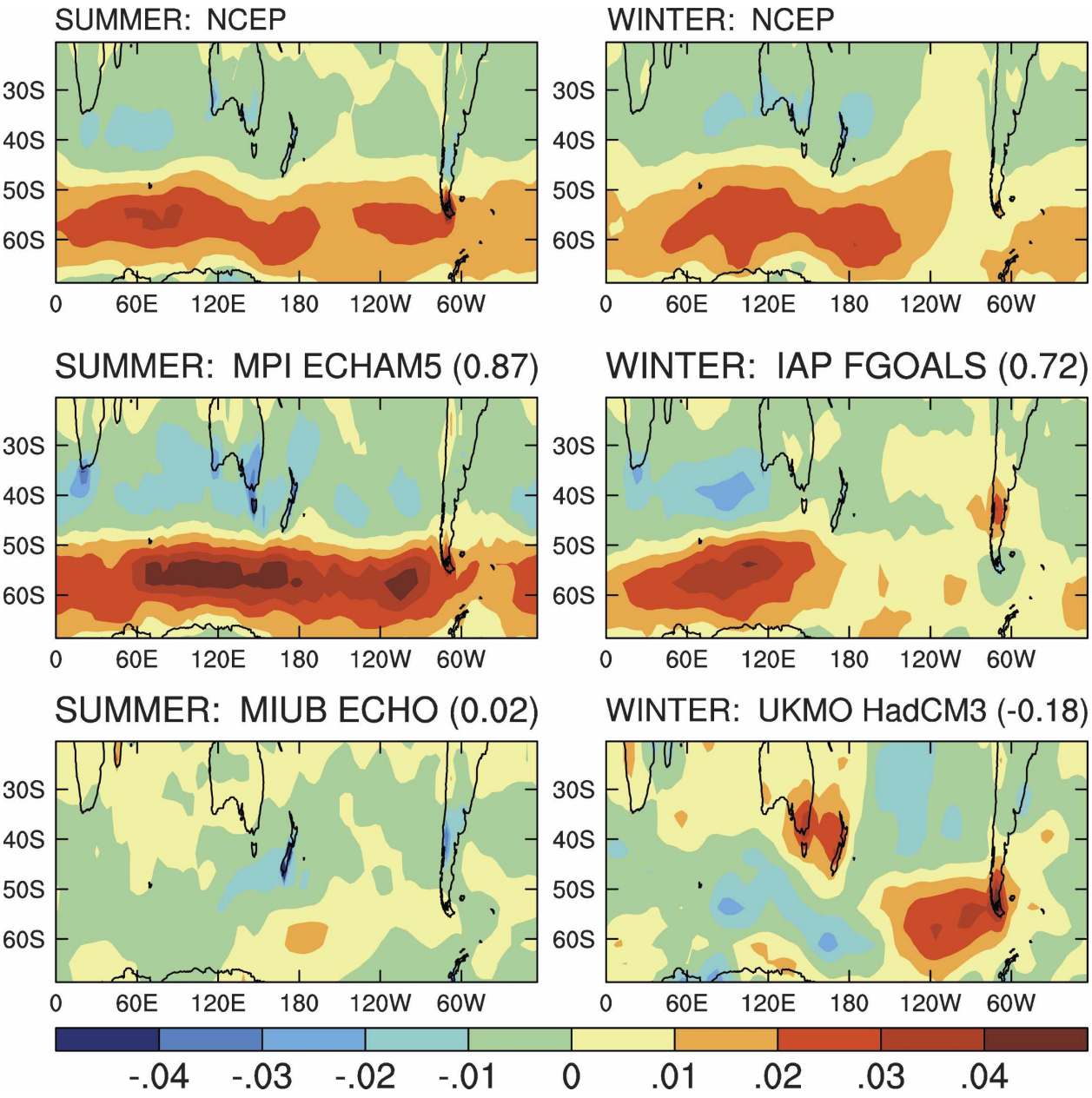

FIG. 3. Samples of trend patterns from models that have high and low pattern correlation coefficients with the NCEP trend pattern for (left column) DJF and(right column) JJA. Model units: N m^{-2} per half century (1950–99); NCEP units: N m^{-2} per 43 yr (1957–99). Pattern correlations with NCEP trend pattern are in brackets next to model name.

structure because the EOF analysis appears to be rather effective in picking up the SAM, which is zonally symmetric. This feature is elucidated in Fig. 7 in a comparison of EOF1 patterns from models with high [Meteorological Research Institute Coupled General Circulation Model version 2 (MRI CGCM2)], medium [GFDL Climate Model version 2.0 (GFDL CM2.0)], and low [L'Institut Pierre-Simon Laplace Coupled Model version 4 (IPSL CM4)] correlation coefficients. The center of action in the IPSL CM4 model is located much farther north than that in the MRI CGCM2 model.

2) STATISTICAL SIGNIFICANCE OF TRENDS IN EOF1

Trends and the statistical significance of the EOF1 time series from each model are calculated and compared in Fig. 8. Except for GISS AOGCM and Meteorological Institute of the University of Bonn (MIUB)

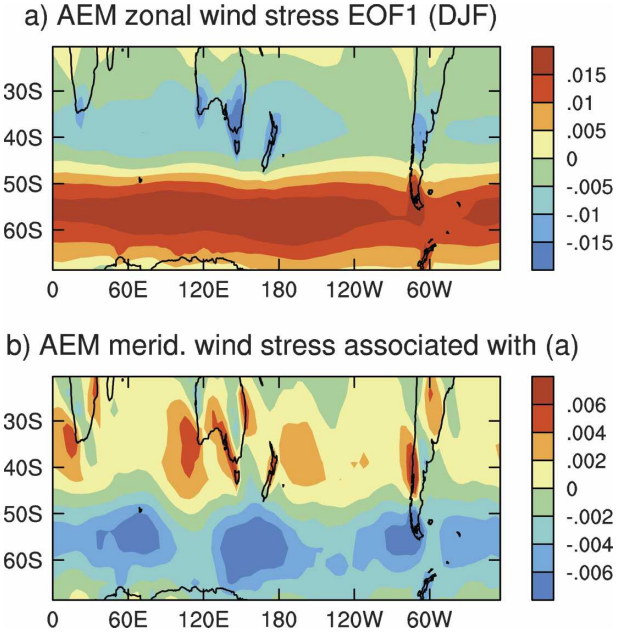

FIG. 4. (a) AEM pattern of trends in EOF1 of DJF zonal wind stress in each model, and (b) the associated meridional wind stress pattern. Units: N m^{-2} per half century (1950–99). The trend in each model is obtained by multiplying the spatial pattern with the slope of the EOF1 time series.

ECHAM4 Hamburg Ocean Primitive Equation (ECHO-G), which display a negative and near-zero trend, respectively, all models show a bias toward a positive trend of the SAM. However, there is a wide spread in the magnitude of the trend and the differences are rather high. These features are partially reflected in the trend analysis of section 3a.

To assess the significance of these trends, long-

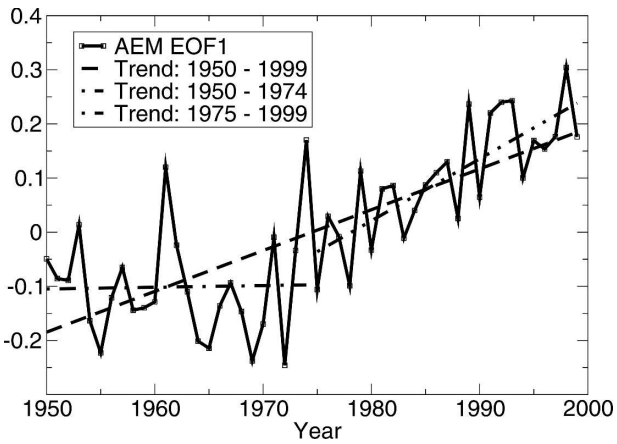

FIG. 5. AEM time series of EOF1 from individual models. Superimposed are trend lines for the full period, for 1950–74 and for 1975–99, which are 0.38, 0.016, and 0.57 per half century, respectively.

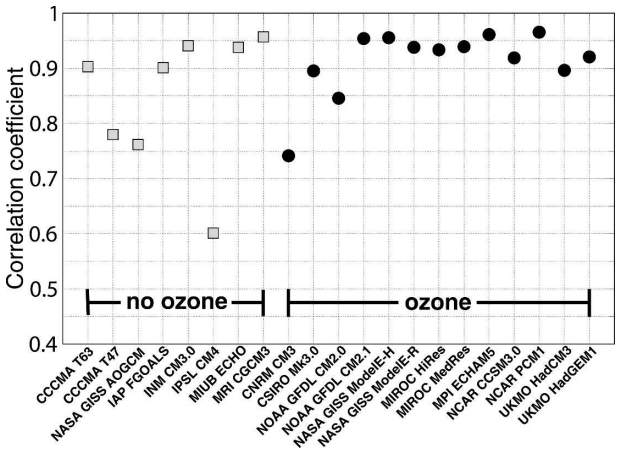

FIG. 6. Pattern correlation between zonal wind stress EOF1 from individual models and that shown in Fig. 4a.

control (without external forcing) experiments are needed to estimate the range of 50-yr trends due to natural variability of the coupled climate system. To this end, we employed a 500-yr-long control run from the Commonwealth Scientific and Industrial Research Organisation Mark version 3.0 (CSIRO Mk3.0) and GFDL CM2.1 models in DJF. Outputs from both models are interpolated onto the same grid, and EOF analysis on zonal wind stress is carried out. The EOF pattern is, as expected, similar to that shown in Fig. 4a. Time series of the 50-yr trends from each model are obtained using a moving 50-yr window on the TAF. The standard deviation of the 50-yr trend is 0.27 for the CSIRO Mk3.0 and 0.26 for the GFDL CM2.1, that is, virtually identical. Assuming that every model and the observed has a similar amplitude of variations of 50-yr trends from natural variability, the sigma value (taken as 0.27) is used to estimate the uncertainty range taking into account the ensemble member, following the approach of Marshall et al. (2004). The results show that the trends in the majority of models (15 out of 21 models) are statistically significant as displayed in Fig. 8. As a whole, the AEM produces a SAM-like trend that is statistically significant. The trend obtained from an all model average, regardless of a model's ensemble member, is comparable to that of the AEM (not shown).

Six models produce trends that are not statistically significant, including the GISS AOGCM, which yields a negative trend. It so happens that none of these six models includes ozone forcing, supporting the importance of ozone in generating the trends in the other models. Canadian Centre for Climate Modelling and Analysis (CCCma) T47 and MRI CGCM2 stand out as exceptions; without ozone depletion, they generate sizable, significant trends. On the other hand, the seven

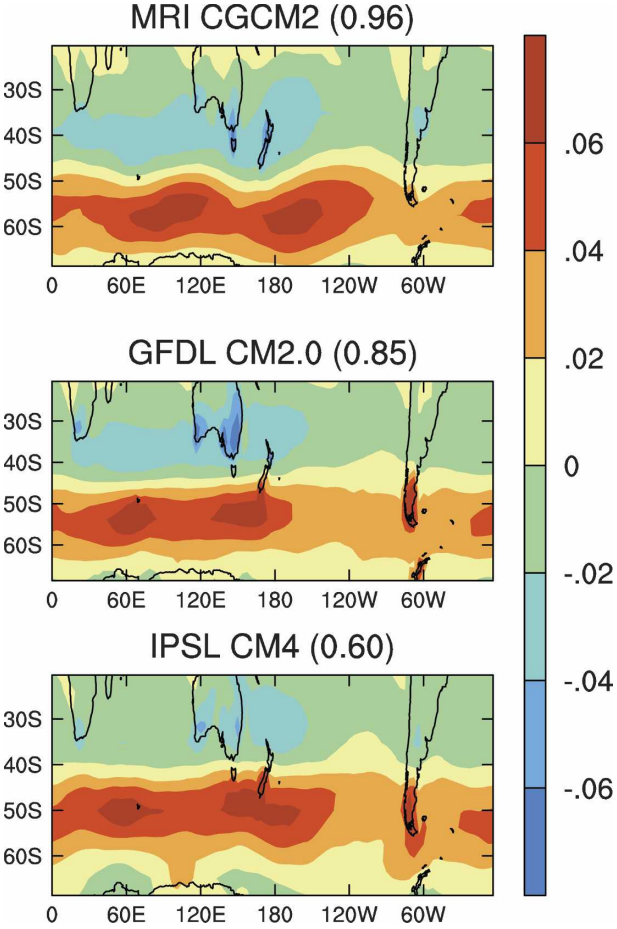

FIG. 7. Samples of DJF zonal wind stress EOF1 patterns of models having high, medium, and low pattern correlation coefficients with that shown in Fig. 4a; correlations are in brackets next to model name.

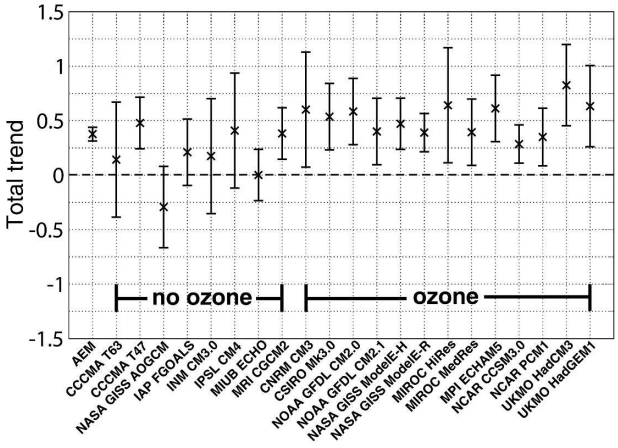

FIG. 8. Total trends and statistical significance test for AEM EOF1 (Fig. 5) and individual models over 1950–99. For each model the trend is derived from the ensemble mean of the model. The error bars are estimated using zonal wind stress EOF1 time series from two 500-yr control (without external forcing) experiments, one from CSIRO Mk3.0, and one from GFDL CM2.1, which yields essentially identical standard deviation in 50-yr-long trend.

strongest trends come from models that include ozone depletion. We shall discuss the relative importance of ozone and greenhouse warming in section 4.

4. Discussion

a. Comparison with observations

As alluded to in the introduction, NCEP reanalysis produces a SAM trend in terms of MSLP that is too strong. It follows that the trend in zonal wind stress EOF1 will be too strong as zonal wind and MSLP are basically in geostrophic balance. As discussed in section 2 we correct this bias by regressing NCEP wind stress onto the observed station-based index of the SAM (Marshall 2003). The EOF1 pattern of the corrected NCEP zonal wind stress, which is identical to the pattern of regression coefficient of zonal wind stress upon the station-based SAM index, is used to benchmark model performance (Fig. 9). The results show the AEM EOF1 scores the highest, highlighting the advantage of a multimodel, multiexperiment ensemble strategy in alleviating model errors. In general, the majority of models correlate highly with the NCEP EOF1, with 9 out of the top 12 models from the ozone group.

Assuming that the real climate system without external forcing has a similar level of variability to that in the 500-yr control runs of CSIRO Mk3.0 and GFDL CM2.1, the statistical significance of the trend in the

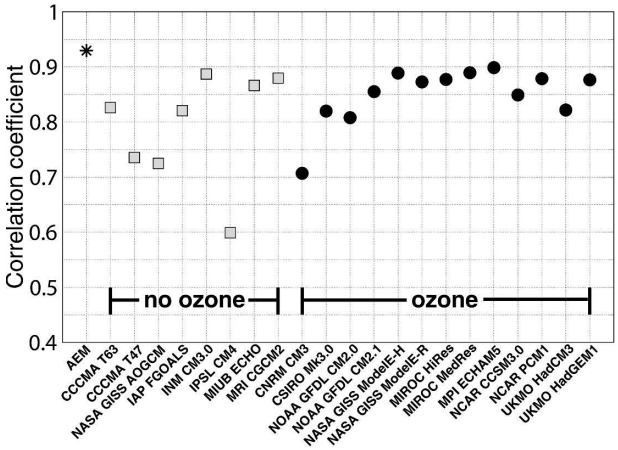

FIG. 9. Pattern correlation between EOF1 from corrected NCEP zonal wind stress with EOF1 of zonal wind stress from individual models and AEM, shown in Fig. 4a, over the period 1950–99. The NCEP zonal wind stress is corrected using a station-based, non-normalized SAM index of Marshall (2003).

EOF1 of the corrected NCEP zonal wind stress is tested and the result is shown in Fig. 10 together with the AEM EOF1. The trend in EOF1 from the corrected NCEP zonal wind stress is marginally significant. The trend in AEM is more than two-thirds (0.38 ± 0.06 N m^{-2}) of the trend from the corrected NCEP (0.53 ± 0.52 N m^{-2}). However, the trend in the group with ozone-depletion forcing produces a trend of 0.45 ± 0.08 N m^{-2}, which compares reasonably well with the corrected NCEP, given the large uncertainty range.

b. The impact of ozone depletion

As mentioned previously, we divided the model experiments into two categories: those with and without ozone-depletion forcing. The total number of experiments with ozone forcing is 48 and the total number without ozone is 23. The trends in each group are significant as they are obtained from a large number of experiments. Two central results emerge from Fig. 10. First, modeled trends are in better agreement when ozone depletion (0.45 ± 0.08 N m^{-2}) is included; however, errors in the observed NCEP are large (0.53 ± 0.52 N m^{-2}). Second, without ozone depletion, the trend (0.22 ± 0.11 N m^{-2}) is less than half of the total trend in the models, suggesting that although the contribution by ozone might be underestimated in the models, it still accounts for more than half of the total trend in the models. The importance of ozone depletion is further highlighted by the feature that the trend commences from the mid-1970s when ozone started to deplete significantly (Fig. 5); prior to the mid-1970s there is little trend.

c. Implied ocean circulation changes

There are even fewer observations to assess the changes to the subtropical gyre circulation, but this can be estimated from well-established wind-driven ocean circulation theory (Stommel 1948). It is the wind stress curl, not the wind stress, that is important for the large-scale gyre circulation. Wind stress curl from the corrected NCEP and from the set of experiments with forcing of ozone depletion displays a comparable trend (Fig. 11). The similarity is confirmed by a pattern correlation coefficient of 0.88. Previous studies did not examine the impact on the SH subtropical and midlatitude oceanic circulation probably because the maximum change of zonal wind stress is located far to the south (Fig. 4), at approximately 60°S. The wind stress curl at southern midlatitudes is dominated by the meridional gradient of zonal wind stress. As a result, the center for the maximum wind stress curl change is located at approximately 45°–50°S (Fig. 11), at a latitude able to significantly affect the subtropical gyre circulation. The change is calculated using a well-established wind-driven circulation model, the Island Rule of Godfrey (1989), and is shown in Fig. 12. The main point is

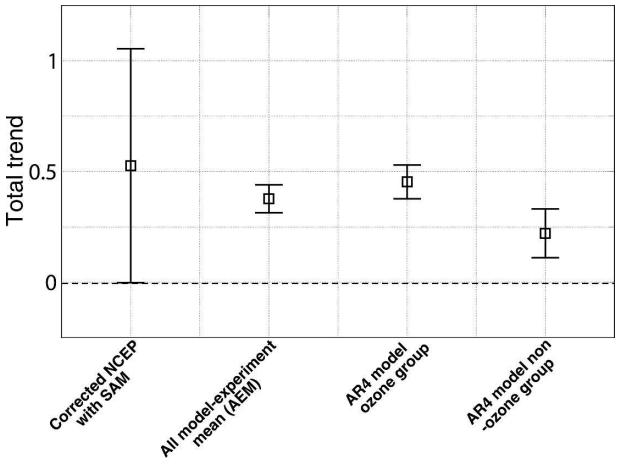

FIG. 10. Total trends and statistical significance test for EOF1 from corrected NCEP zonal wind stress, AEM, and mean over experiments with and without ozone forcing, over the period 1950–99. The error bars are estimated using zonal wind stress EOF1 time series from two 500-yr control (without external forcing) experiments, one from CSIRO Mk3.0, and one from GFDL CM2.1, which yields essentially identical standard deviation in 50-yr-long trend.

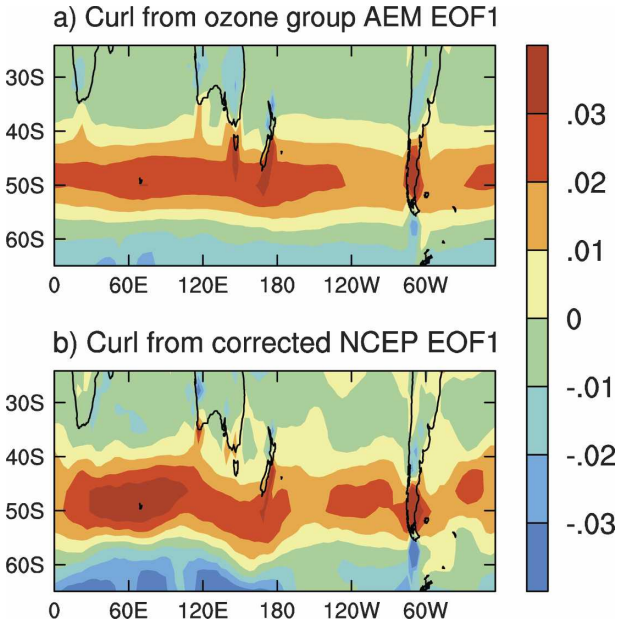

FIG. 11. Total trends in wind stress curl from the mean EOF1 averaged over experiments with ozone-depletion forcing and from EOF1 of the corrected NCEP winds. NCEP units: N m^{-3} per 43 yr (1957–99); model units: N m^{-3} per half century (1950–99); units scaled by 10^{-6}.

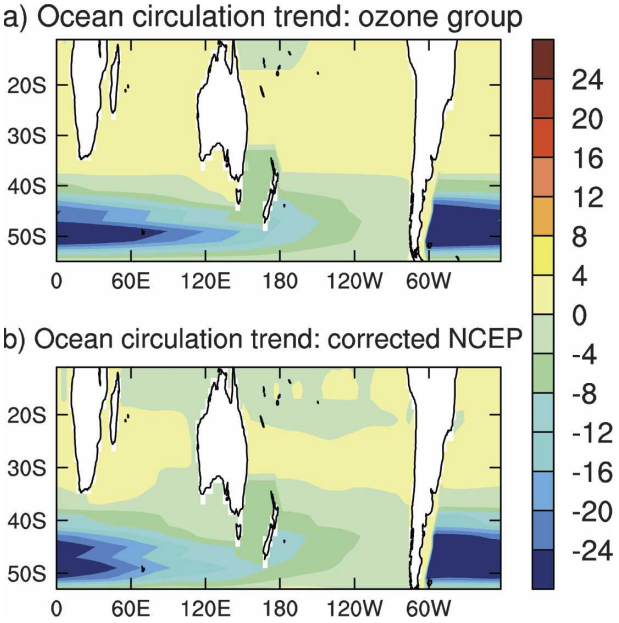

FIG. 12. Total changes to ocean circulation associated with trends shown in Fig. 11: (a) from models with forcing of ozone depletion and (b) from corrected NCEP. The changes are calculated using Godfrey's (1989) Island Rule model; Units: Sv.

that the change to the subtropical gyre circulation is an integrated effect of the curl change from an eastern boundary, which is different from previous analyses focusing on the direct and local effect of zonal wind changes.

The oceanic circulation trend calculated from the curl in the models with ozone-depletion forcing (Fig. 12a) and from the corrected NCEP curl (Fig. 12b) compares well: the overall pattern is similar and includes a southward shift and spinup of the Southern Ocean supergyre linking the subtropical South Pacific, Indian, and Atlantic Ocean circulation (Cai 2006). The largest changes occur in the South Atlantic because of the pan-circumpolar integration of the wind stress curl from the eastern boundary to the western boundary of South America. The circulation change includes a strengthening of the East Australian Current flow (about 8 Sv; 1 Sv = 10^6 m^3 s^{-1}) passing through the Tasman Sea. Cai (2006) argues that Antarctic ozone depletion is mainly responsible for a similar Southern Ocean circulation change since the late 1970s. This appears to be supported by the AR4 models, as Fig. 5 illustrated that most of the trend commences since mid-1970s. Cai (2006) further suggested that as the intensifying gyres advect more warmed water, they contribute to the observed unusually large warming in the midlatitude Southern Ocean (Gille 2002) and to the reported range extension to the south of many marine species in the southwest Pacific (Pittock 2003).

5. Conclusions

We have assessed the simulation by 21 IPCC AR4 models of DJF circulation trends in the SH over the period of 1950–99, focusing on the trend that is congruent with the SAM in terms of surface zonal wind stress. The main results are as follows.

- The total trend is principally congruent with the model SAM trend, as in observations.
- In terms of trend pattern, results from the AEM achieve a correlation with that from the corrected NCEP higher than all individual models.
- The majority of models produce a statistically significant positive trend (with decreasing westerlies in midlatitudes and increasing westerlies in high latitudes) and only one model produces a negative trend.
- All model trends that are not statistically significant are from models that *do not* include ozone-depletion forcing.
- Models with ozone-depletion forcing, as well as greenhouse forcing, produce an averaged trend that is more than twice as large as that in models without ozone-depletion forcing.
- Only with ozone-depletion forcing do models produce an averaged trend that is close to the corrected NCEP trend; however, errors in the observed trend are large.
- The trend is largely generated after the mid-1970s in both the corrected NCEP data and the AR4 models, when ozone started to deplete significantly.
- The impact on oceanic circulation change shows an intensification of the SH supergyre circulation, including a strengthening flow through the Tasman Sea.

Synthesizing these results, we conclude that AR4 models as an entity realistically simulate the pattern of change of the SH circulation, and with the inclusion of ozone-depletion forcing the trend is close to the corrected NCEP. These models support the consensus that Antarctic ozone depletion plays a significant part in driving the SH climate change and involves a mechanism from the stratosphere to the ocean.

Acknowledgments. This work is part of the CSIRO Wealth from Oceans Flagship and is supported by the Australian Greenhouse Office. We thank Gareth Marshall for the station-based SAM index and Ian Smith and the three anonymous external reviewers for the helpful and insightful comments. In addition, we acknowledge the work undertaken by numerous international modeling groups who provided their model experiments for analysis. In particular we recognize the

significant work that the U.S. Department of Energy's Program for Climate Model Diagnosis and Intercomparison (PCMDI) has achieved in collecting and storing the model data. For more details on model data or documentation, readers are referred to the PCMDI Web site (http://www-pcmdi.llnl.gov).

REFERENCES

Arblaster, J. M., and G. A. Meehl, 2006: Contributions of external forcings to southern annular mode trends. *J. Climate,* **19,** 2896–2905.

Cai, W., 2006: Antarctic ozone depletion causes an intensification of the Southern Ocean super-gyre circulation. *Geophys. Res. Lett.,* **33,** L03712, doi:10.1029/2005GL024911.

——, P. H. Whetton, and D. J. Karoly, 2003: The response of the Antarctic Oscillation to increasing and stabilized atmospheric CO_2. *J. Climate,* **16,** 1525–1538.

——, G. Shi, T. Cowan, D. Bi, and J. Ribbe, 2005: The response of the southern annular mode, the East Australian Current, and the southern midlatitude ocean circulation to global warming. *Geophys. Res. Lett.,* **32,** L23706, doi:10.1029/2005GL024701.

Carril, A. F., C. G. Menéndez, and A. Navarra, 2005: Climate response associated with the southern annular mode in the surroundings of Antarctic Peninsula: A multimodel ensemble analysis. *Geophys. Res. Lett.,* **32,** L16713, doi:10.1029/2005GL023581.

Collins, W. D., and Coauthors, 2006: Radiative forcing by well-mixed greenhouse gases: Estimates from climate models in the IPCC AR4. *J. Geophys. Res.,* **111,** D14317, doi:10.1029/2005JD006713.

Delworth, T. L., and Coauthors, 2006: GFDL's CM2 global coupled climate models. Part I: Formulation and simulation characteristics. *J. Climate,* **19,** 643–674.

Diansky, N. A., and E. M. Volodin, 2002: Simulation of present-day climate with a coupled atmosphere–ocean general circulation model. *Izv. Atmos. Oceanic Phys.,* **38,** 732–747.

Flato, G. M., G. J. Boer, W. G. Lee, N. A. McFarlane, D. Ramsden, M. C. Reader, and A. J. Weaver, 2000: The Canadian Centre for Climate Modeling and Analysis global coupled model and its climate. *Climate Dyn.,* **16,** 451–467.

Fyfe, J. C., and O. A. Saenko, 2005: Human-induced change in the Antarctic Circumpolar Current. *J. Climate,* **18,** 3068–3073.

——, and ——, 2006: Simulated changes in the extratropical Southern Hemisphere winds and currents. *Geophys. Res. Lett.,* **33,** L06701, doi:10.1029/2005GL025332.

——, G. J. Boer, and G. M. Flato, 1999: The Arctic and Antarctic Oscillations and their projected changes under global warming. *Geophys. Res. Lett.,* **26,** 1601–1604.

Gille, S. T., 2002: Warming of the Southern Ocean since the 1950s. *Science,* **295,** 1275–1277.

Gillett, N. P., and D. W. J. Thompson, 2003: Simulation of recent Southern Hemisphere climate change. *Science,* **302,** 273–275.

Godfrey, J. S. A., 1989: Sverdrup model of the depth-integrated flow for the World Ocean allowing for island circulations. *Geophys. Astrophys. Fluid Dyn.,* **45,** 89–112.

Gordon, C., C. Cooper, C. Senior, H. Banks, J. Gregory, T. Johns, J. Mitchell, and R. Wood, 2000: The simulation of SST, sea ice extents and ocean heat transports in a version of the Hadley Centre coupled model without flux adjustments. *Climate Dyn.,* **16,** 147–168.

Gordon, H. B., and Coauthors, 2002: The CSIRO Mk3 Climate System Model. CSIRO Atmospheric Research Tech. Rep. 60, 130 pp.

Hartmann, D. L., and F. Lo, 1998: Wave-driven zonal flow vacillation in the Southern Hemisphere. *J. Atmos. Sci.,* **55,** 1303—1315.

Hasumi, H., and S. Emori, 2004: K-1 coupled GCM (MIROC) description. K-1 Tech. Rep. 1, Center for Climate System Research (CCSR), University of Tokyo, 34 pp.

Johns, T., and Coauthors, 2005: HadGEM1—Model description and analysis of preliminary experiments for the IPCC Fourth Assessment Report. Tech. Rep. 55, Hadley Centre, 74 pp.

Jungclaus, J. H., and Coauthors, 2006: Ocean circulation and tropical variability in the coupled model ECHAM5/MPI-OM. *J. Climate,* **19,** 3952–3972.

Kalnay, E., and Coauthors, 1996: The NCEP/NCAR 40-Year Reanalysis Project. *Bull. Amer. Meteor. Soc.,* **77,** 437–471.

Karoly, D. J., 1990: The role of transient eddies in low-frequency zonal variations of the Southern Hemisphere circulation. *Tellus,* **42A,** 41–50.

Kidson, J. W., 1988: Interannual variations in the Southern Hemisphere circulation. *J. Climate,* **1,** 1177–1198.

Kushner, P. J., I. M. Held, and T. L. Delworth, 2001: Southern Hemisphere atmospheric circulation response to global warming. *J. Climate,* **14,** 2238–2249.

Legutke, S., and R. Voss, 1999: The Hamburg atmosphere–ocean coupled circulation model ECHO-G. Tech. Rep. 18, German Climate Computing Centre (DKRZ), 62 pp.

Marshall, G. J., 2003: Trends in the southern annular mode from observations and reanalyses. *J. Climate,* **16,** 4134–4143.

——, P. A. Scott, J. Turner, W. M. Connolley, J. C. King, and T. A. Lachlan-Cope, 2004: Causes of exceptional atmospheric circulation changes in the Southern Hemisphere. *Geophys. Res. Lett.,* **31,** L14205, doi:10.1029/2004GL019952.

Marti, O., and Coauthors, 2005: The new IPSL climate system model: IPSL-CM4. Note du Pôle de Modélisation 26, IPSL, 84 pp.

Meehl, G. A., and Coauthors, 2006: Climate change projections for the twenty-first century and climate change commitment in the CCSM3. *J. Climate,* **19,** 2597–2616.

Miller, R. L., G. A. Schmidt, and D. T. Shindell, 2006: Forced annular variations in the 20th century Intergovernmental Panel on Climate Change Fourth Assessment Report models. *J. Geophys. Res.,* **111,** D18101, doi:10.1029/2005JD006323.

Pittock, B., 2003: *Climate Change: An Australian Guide to the Science and Potential Impacts*. Australian Greenhouse Office, 239 pp.

Randel, W. J., and F. Wu, 1999: Cooling of the Arctic and Antarctic polar stratospheres due to ozone depletion. *J. Climate,* **12,** 1467–1469.

Raphael, M. N., and M. M. Holland, 2005: Twentieth century simulation of the Southern Hemisphere in coupled models. Part I: Large scale circulation variability. *Climate Dyn.,* **26,** 217–228.

Russell, G. L., J. R. Miller, and D. Rind, 1995: A coupled atmosphere–ocean model for transient climate change studies. *Atmos.–Ocean,* **33,** 683–730.

Russell, J. L., K. W. Dixon, A. Gnanadesikan, R. J. Stouffer, and J. R. Toggweiler, 2006a: The Southern Hemisphere westerlies in a warming world: Propping open the door to the deep ocean. *J. Climate,* **19,** 6382–6390.

——, R. J. Stouffer, and K. W. Dixon, 2006b: Intercomparison of

the Southern Ocean circulations in the IPCC coupled model control simulations. *J. Climate,* **19,** 4560–4575.

Schmidt, G. A., and Coauthors, 2006: Present-day atmospheric simulations using GISS ModelE: Comparison to in situ, satellite, and reanalysis data. *J. Climate,* **19,** 153–192.

Sexton, D. M. H., 2001: The effect of stratospheric ozone depletion on the phase of the Antarctic oscillation. *Geophys. Res. Lett.,* **28,** 3697–3700.

Shindell, D. T., and G. A. Schmidt, 2004: Southern Hemisphere climate response to ozone changes and greenhouse gas increases. *Geophys. Res. Lett.,* **31,** L18209, doi:10.1029/2004GL020724.

Solomon, S., R. W. Portmann, T. Sasaki, D. J. Hofman, and D. W. J. Thompson, 2005: Four decades of ozonesonde measurements over Antarctica. *J. Geophys. Res.,* **110,** D21311, doi:10.1029/2005JD005917.

Stommel, H., 1948: The westward intensification of wind driven ocean currents. *Eos, Trans. Amer. Geophys. Union,* **29,** 202–206.

Thompson, D. W. J., and S. Solomon, 2002: Interpretation of recent Southern Hemisphere climate change. *Science,* **296,** 895–899.

——, J. M. Wallace, and G. C. Hegerl, 2000: Annular modes in the extratropical circulation. Part II: Trends. *J. Climate,* **13,** 1018–1036.

Washington, W. M., and Coauthors, 2000: Parallel climate model (PCM) control and transient simulations. *Climate Dyn.,* **16,** 755–774.

Waugh, D. W., W. J. Randel, S. Pawson, P. A. Newman, and E. R. Nash, 1999: Persistence of the lower stratospheric polar vortices. *J. Geophys. Res.,* **104,** 27 191–27 202.

Yin, J. H., 2005: A consistent poleward shift of the storm tracks in simulations of 21st century climate. *Geophys. Res. Lett.,* **32,** L18701, doi:10.1029/2005GL023684.

Yu, Y., Z. Xuehong, and G. Yufu, 2004: Global coupled ocean–atmosphere general circulation models in LASG/IAP. *Adv. Atmos. Sci.,* **21,** 444–455.

Yukimoto, S., A. Noda, S. Uchiyama, T. Kusunoki, and A. Kitoh, 2005: Climate changes of the twentieth through twenty-first centuries simulated by the MRI-CGCM2.3. *Pap. Meteor. Geophys.,* **56,** 9–24.

Zhou, S. T., M. E. Gelman, A. J. Miller, and J. P. McCormack, 2000: An inter-hemisphere comparison of the persistent stratospheric polar vortex. *Geophys. Res. Lett.,* **27,** 1123–1126.